

A System Analysis of Error Sources in the Technique Used for Ionospheric Calibration of Deep Space Probe Radio Metric Data

K. W. Yip and B. D. Mulhall
Tracking and Orbit Determination Section

A system analysis has been performed on the error sources in the technique used for ionospheric calibration of deep space probe radio metric data. This analysis is based on the Chapman ionospheric model. Although it has been proven that this model is inadequate in ranging for low elevation angles ($\lesssim 15$ deg) of the spacecraft and large solar zenith angles ($\gtrsim |60|$ deg), this analysis should still be valid for most of the daytime because of the very conservative values adopted for the variations of these Chapman ionospheric parameters. It is found that if a close-by source of total electron content (TEC) data is used, the uncertainty is $\sim 10\%$ at low elevation angles and less than $\sim 3\%$ for elevation angles higher than ~ 20 deg. The corresponding values for the distant mapping of TEC data are $\sim 10\%$ and $\sim 8\%$, respectively.

I. Introduction

The charged particles in the ionosphere and the interplanetary space plasma along the ray path of the radio signal transmitted to and received from a spacecraft have various effects upon the signal. The two effects which concern orbit determination are the phase path decrease and group path delay. This increase in phase velocity and decrease in group velocity is a function of the wave frequency; thus the plasma has a dispersive effect on the spectrum of the radio signal.

As the number of charged particles along the ray path changes, the phase path changes and shifts the transmitted carrier frequency. This frequency shift cannot be distinguished from the doppler effect unless the change

in the number of charged particles is determined. Similarly, the charged particles delay the energy of the transmitted radio signal, a result that increases the round-trip light time of this signal and therefore corrupts range data, since these measurements are based on the time required for the energy to propagate from the tracking station to the spacecraft and return.

The ionosphere causes two types of navigational errors: random and systematic. Random errors in the doppler observable can be reduced by taking data over many passes. Systematic errors cannot be reduced by averaging. If the systematic error is essentially constant over each pass, it will corrupt the estimate of geocentric range rate, the parameter a of the Hamilton-Melbourne model

(Ref. 1), rather than station location. However, if the error is a time-varying function with a diurnal period, then estimates of station spin radius r_s will be corrupted by antisymmetric (odd) errors, and station longitude λ by symmetric (even) errors.

Earth's ionosphere is caused by ultraviolet radiation from the Sun ionizing the upper atmosphere. Consequently, the density of charged particles in the ionosphere increases and decreases with a diurnal period. For post-flight analysis (Ref. 2), the diurnal variation of the ionosphere will corrupt the station location estimates. For in-flight orbit determination, the ionospheric effect will corrupt the estimate of the probe's orbit.

The quantity most important in the determination of ionospheric effect is the total electron content (TEC) along the line of sight to the spacecraft:

$$I(t) = \int_0^S N(s, t) ds \quad (1)$$

where $N(s, t)$ is the electronic distribution along the ray path S at time t . This is related to the corresponding range change by the equation

$$\Delta\rho(t) = \frac{A}{f^2} I(t) \quad (2)$$

where $A = 40.3$ in mks units, and f is the transmitted frequency in hertz.

Figure 1 is a block diagram of the steps involved in the ionospheric calibration technique described in this article. The details of this approach have been well documented in Ref. 3. The discussions in the following sections are divided according to these steps, with more emphasis placed on the error analyses. The results of these analyses in terms of the line-of-sight one-way range changes in the spacecraft view period are tabulated in Table 1.

II. Recapitulation of the Ionospheric Calibration Technique

For the convenience of the reader, a brief summary of the entire calibration technique is made here.

Since the idea of the "ionospheric reference point" is going to come up again and again in the following discussion, it is appropriate to familiarize the reader with this concept. This point is defined as the point where the

radio signal ray path passes a reference altitude, namely, 350 km (Ref. 3). This reference altitude is also the height which best satisfies the "thin shell approximation" (Ref. 4) in the Faraday data reduction. Ionospheric conditions at this point are used to typify conditions along the entire ray path.

As shown in Fig. 1, the ionospheric data come either from ionosonde measurements or Faraday rotation observations to geostationary satellites. Ionosonde data are measured vertically from the station and, as a result, information at the zenith of the station is obtained. Faraday rotation measurements, on the other hand, yield data along the line of sight to the geostationary satellite. To be compatible with ionosonde TEC, these Faraday values are multiplied by the cosine of the angle between the zenith at the reference point (Ref. 3) and the ray path. Consequently, ionosonde and Faraday rotation data can be mapped in exactly the same manner, the only difference being that the Faraday rotation data are related to a point under the slanted column, rather than the zenith of the monitoring station.

To calibrate range changes due to ionospheric effects, the program takes in the diurnal variations of the zenith TEC for the days when calibrations are required. Of course, if there are periods in the TEC data spans where no data are available, no calibration can be performed for the corresponding periods. (This assumes that no model for the TEC data is to be used. There is, however, a capability in the program in cases when the model data are desired. A description of the evaluation of these diurnal models is given in Ref. 5.) Usually, the locations of the ionospheric observatories and the tracking stations are different and space-time translations (Ref. 3) of the zenith TEC are required. After these zenith TEC values are mapped to the tracking station, they are re-converted to the line-of-sight (to the spacecraft) values by the ray-trace technique (Ref. 6). The corresponding range changes due to the ionosphere are then computed from Eq. (2), together with the geomagnetic latitude adjustment factor (Ref. 3). These range functions $\Delta\rho(t)$ are fitted by polynomials in time, and the coefficients are then used for the computations of range changes and range rates at any time during the respective passes when the TEC data are available.

This one-way range change can be used as a calibration by the Orbit Determination Program (ODP) or this calibration program can convert it to a doppler calibration. The doppler calibration can be obtained either by taking the time derivative of the one-way range polynomial or by the "four-path differencing" technique. This latter

method takes into account the fact that we are calibrating two-way doppler which has been differenced over the count time. The details of this approach have been outlined in Ref. 3 and are not repeated here.

III. Error Sources

The different stages in the ionospheric calibration technique (see Fig. 1) where possible errors may occur are:

- (1) Instrumentation errors such as equipment noise which are however negligible.
- (2) Computing zenith TEC from ionosonde or Faraday rotation measurements.
- (3) Performing the space-time translation of these data.
- (4) Converting from zenith TEC to TEC along the desired lines of sight.
- (5) Curve fitting of the range change values.
- (6) Computing doppler calibration.
- (7) Curve fitting of doppler values.

Before going any further, it should be mentioned that all of the following analyses are based on a Chapman ionosphere (Ref. 7). In other words, the electronic distribution of the ionosphere is given by

$$N(z) = N_{\max} \exp \left\{ \frac{1}{2} \left(1 - z - \frac{1}{\cos \chi} e^{-z} \right) \right\} \quad (3)$$

where

$$z = (h - H_{\max})/B$$

h = altitude above Earth

H_{\max} = altitude above Earth where the peak electron density occurs

N_{\max} = maximum electron density (occurring at H_{\max})

B = scale height of ionosphere

χ = solar zenith angle

This is a good representation of the ionospheric distribution in relation to range calibration in the daytime for not too small elevation angles (≥ 15 deg) and not too large solar zenith angles ($\leq |60|$ deg) (see Ref. 8).

Since this equation is the basis for some of the major operations in this ionospheric calibration scheme, strictly speaking, this error analysis is relevant only to range

calibrations in the daytime and within the range of angles just mentioned. However, in spite of the fact that in some of the following analyses the ranges of angles are exceeded, it is felt that these estimates are still valid for most of the daytime, all the more so since very conservative values have been adopted for the variations of these Chapman ionospheric parameters.

A. Instrumental Errors

Since the ionosonde data are supplied by external sources and their instrumental errors are difficult to ascertain exactly, the analysis is primarily concerned with the Faraday rotation measurements. Fortunately, except for some early missions, this data source is used almost exclusively. From an experiment performed some time ago (Ref. 9), the equipment noise is found to be about three orders of magnitude below the signal level. Thus, it is valid to conclude that there is no error associated with the value of the Faraday rotated angle Ω .

B. Computation of Zenith TEC

1. **Computation from ionosonde data.** Basically, the ionosonde measurement involves the analysis of radar-like echoes from the ionosphere over a wide range of operating frequencies (Ref. 10). As long as there is a reflection from the ionosphere, this particular frequency is related to the density at this height h (derived from the "virtual" height (Ref. 10) computed from the time of flight of this echo) by

$$N = Af^2 \quad (4)$$

where $A = 1.24 \times 10^{-2}$ electrons/m³/Hz²; N = density of electrons, electrons/m³; and f = reflected frequency, Hz. At some frequency ($f_0 F2$), however, the signal pierces through the ionosphere. Thus, only $N(h)$ for the lower ionosphere can be obtained. For the upper ionosphere, therefore, assumptions for the electronic profile and scale height (Ref. 3) have to be made. This is where most of the uncertainties come in, since this upper portion of the ionosphere past the $F2$ peak contains the majority (>75%) of the electrons. This is the basis for the authors' opinion that errors in ionosonde data are probably the cause for apparent disagreement between Faraday rotation and ionosonde measurements when the two data types are compared.

2. Computation from Faraday rotation data

a. *Conversion from raw measurements to TEC.* The reduction of the Faraday rotation measurements involves

the “thin shell approximation” (Ref. 4). Instead of the actual Faraday rotation equation

$$\Omega = \frac{R}{f^2} \int_0^S \|H\| \cos \theta(s) N(s) ds \quad (5)$$

where

Ω = Faraday rotation of polarization vector
(with π ambiguities removed), rad

$R = 2.97 \times 10^{-2}$, mks units

f = transmitted frequency, Hz

S = ray path to satellite, m

$\|H\| \cos \theta$ = tangential component of Earth’s magnetic field at a reference point along ray path, A-t/m

$N(s)$ = electron density at point s along ray path, electrons/m³

the “thin shell” approximation involves picking an appropriate value for the quantity $\|H\| \cos \theta$ and then pulling it outside of the integral. In other words,

$$\Omega = \frac{R}{f^2} \langle \|H\| \cos \theta \rangle_{\text{ref alt}} \int_0^S N(s) ds = \frac{R}{f^2} \langle \|H\| \cos \theta \rangle_{\text{ref alt}} I \quad (6)$$

and I , of course, is the TEC along this particular line of sight. The subscript “reference altitude” refers to the altitude along the ray path where the tangential component of Earth’s magnetic field will best satisfy the above equality. A constant reference altitude of 350 km has been used.

The first question concerns itself with the validity of picking a constant reference altitude for the whole day, and, if this is valid, what is the best value to use. An analysis in this respect has already been performed using a Chapman ionosphere (Ref. 11). It is found that with the Chapman parameters of B (scale height) = 39 km, $H_{\text{max}} = 300$ km, and $N_{\text{max}} = 5 \times 10^6$ electrons/cm³, the reference altitude remains constant at 350 ± 25 km irrespective of the elevation angle and direction of the ray path and the solar zenith angle (as long as this is less than ~ 60 deg). Therefore, at Goldstone (colatitude = 57.4 deg),

$$\cos \chi = 0.5388 \sin \delta + 0.8425 \cos \delta \cos \phi \quad (7)$$

and even near dusk or dawn ($|\phi| \cong \pi/2$), the value of χ is ≤ 60 deg. It should be noticed that when χ approaches $\pi/2$, the parameters for the Chapman ionosphere inevitably

vary from those given above. As a matter of fact, it becomes questionable whether a Chapman ionosphere is a good representation at all. An analysis is now under way for the derivation of a model for the nighttime ionosphere so that a model for the ionosphere both night and day (Refs. 8 and 12) will be obtained. Before this is completed, however, the analysis carried out here will give an accurate picture for most of the daytime. A similar analysis for the nighttime including the dawn and dusk transition zones will be performed as soon as the completed model becomes available.

Though a constant reference altitude (for a fixed set of Chapman parameters) is a valid concept to use, the values of the parameters may vary during the day, thus causing the reference altitude to change as well. Figures 2 and 3 show the $\|H\| \cos \theta$ factor as a function of the height in kilometers above Earth for two different orthogonal directions (N–S and E–W). It can be seen that within the reasonable range of reference altitude from 300 to 400 km, the maximum error introduced when one is 50 km off from the “true” altitude is $\sim 2\%$. This estimate is based on a ray path going in the E–W direction, which is reasonable since most of the Faraday rotation data at Goldstone come from observing ATS-1, which is in a westerly direction.

b. Conversion from slant to zenith TEC. Figure 4 shows the geometry of this situation. In the ionospheric calibration program, the conversion is accomplished by taking the cosine of the reference angle α . To be consistent with the eventual translation from zenith to spacecraft line-of-sight TEC values, a “ray-trace” technique should be used in reverse for the elevation angle γ . Tables 2 and 3 illustrate the comparisons between these two approaches for several sets of the Chapman ionospheric parameters, the variations of the solar zenith angle being taken from the July 12, 1965 pass of the Mariner 4 mission and the October 18, 1967 pass of the Mariner 5 mission (see Subsection D and Table 4). The values of H_{max} between 250 and 350 km and B between 29 and 49 km cover the usual range of variations in these parameters as deduced from inspections of ionosonde data. It is seen that for the two different configurations of solar zenith angle variation, the use of the simple cosine introduces errors which are less than 2% for an elevation angle of 35.5 deg. This angle, incidentally, is the value subtended by the line of sight from Goldstone to ATS-1. This error, though small, will be removed in the future version of the program.

C. Space–Time Translation of Zenith TEC

To relate ionospheric measurements to radio tracking data, mapping (or translation in space–time coordinates)

is performed by calculating reference points for both the measurement and the probe-station line of sight. The mapping consists of making use, at one place, the zenith TEC measured at the reference points of another place. This operation is based on the assumption that, at the same local time, two stations have identical zenith TEC values even though they are located quite far apart. This is not exactly true, and the following scheme has been devised to check the uncertainties involved.

A month of zenith TEC in July and in September and October of 1971 from Stanford was time-translated to Goldstone and compared with the zenith TEC measured there in the same periods. Table 5 shows the averages of the daily differences in zenith TEC over a 1/2-h duration and an 8-h span for a whole month. The shorter time span analysis may be more appropriate to VLBI measurements since short-term mapping discrepancies are critical to these observations while the longer time span is appropriate to range corrections for spacecraft tracking. Table 5a gives average discrepancy with the time span centered at 12 noon local time, while Table 5b gives the average discrepancy with the time span centering at 6 p.m. local time. These comparisons give an estimate of the uncertainties involved in "local" (or close-by) mapping of zenith TEC data. Of course, similar analyses for different parts of the year have to be done so that any seasonal variations may be detected. However, without going through lengthy analysis, these comparisons will at least indicate the magnitudes of errors involved when "local mappings" are applied.

For "distant" mapping, the TEC data from Hamilton, Massachusetts, in July and September of 1971 were time-translated to Goldstone and compared. Again, Tables 6a and 6b show averages of the discrepancies for the same daily time spans mentioned above. There are, however, no Massachusetts data available in October for a similar comparison and only the September data have been used.

It should also be noted that if there are any uncertainties involved in the "magnetic latitude" factor (Ref. 3) used in the TEC reduction they would also have been absorbed in the above averages.

An inspection of the daily residuals revealed no definite pattern. In other words, these differences would look like part of a sine function on one day, part of a cosine function on the next, or simply display no trend at all. Since, as mentioned, the station spin radius will be corrupted by odd errors and station longitude by even ones, it is therefore difficult to translate this mapping discrepancy in terms of station location errors.

D. Mapped Zenith TEC to Line of Sight

This analysis is similar to that given in Subsection B-2-b. The elevation angle pertaining to the line of sight, however, is varying during the view period. The calibration proceeds by making use of the following equation to scale the range change at zenith to any arbitrary elevation angles (Ref. 3):

$$R(\gamma) = \frac{\{[(R_e + h_2)^2 - R_e^2 \cos^2 \gamma]^{1/2} - [(R_e + h_1)^2 - R_e^2 \cos^2 \gamma]^{1/2}\}}{(h_2 - h_1)} \quad (8)$$

where

R_e = radius of the Earth, km

γ = elevation angle

h_1 = 215 km

h_2 = 454 km

$R(\gamma)$ is a very good approximation to the ray-trace solution for a Chapman ionosphere with parameters $N_{\max} = 5 \times 10^6$ electrons/cm³, $H_{\max} = 300$ km, and $B = 39$ km, and this expression is normalized to unity at $\gamma = 90$ deg. This factor $R(\gamma)$ is multiplied to the respective "mapped" zenith TEC values to obtain the corresponding TEC and range changes (by Eq. 2) at the different elevation angles in the view period. This approach, however, does not take

into account the effect of the variation of the solar zenith angle in the pass. In other words, in the expression giving the Chapman ionosphere (Eq. 3), χ has been taken to be zero.

As shown in Ref. 13, the range changes for the same elevation angle but different solar zenith angles are quite different. For example, with similar Chapman parameters, the difference in range changes at an elevation angle of 30 deg for $\chi = 0$ deg and $\chi = 34$ deg is almost a meter.

To check this point, ray-trace solutions of the range changes due to a Chapman ionosphere with and without (i.e., $\chi = 0$ deg) solar zenith angle are compared. The numbers in Table 4a are taken from portions of the July 12, 1965 pass of the Mariner 4 mission (Sun-Earth-probe (SEP) angle = 78.1 deg) tracked by DSS 11, while those

in Table 4b are taken from portions of the October 18, 1967 pass of the Mariner 5 mission ($SEP = 48.2$ deg) tracked by the same station. Note that since these are worst-case estimates, the fact that the zenith TEC mapping analysis (step 3, Fig. 1) pertains to the 1971 data while the zenith to line-of-sight analysis pertains to the 1965 and 1967 missions is irrelevant. In Table 4, the elevation angles at the different times of the pass and the corresponding solar zenith angles are tabulated. Tables 7a and b show the corresponding range changes and the ratios $R(\gamma)$ obtained with and without the solar angles. It can be seen that for low elevation angles (≤ 15 deg) and large solar angles (≥ 50 deg), as in the Mariner 5 configuration, the effect of including the solar zenith angle variation in the Chapman expression can cause a deviation of $\geq 2\%$ in the values of the normalized ratio $R(\gamma)$, and thus a similar deviation in the values of the one-way range changes.

These comparisons, however, are based on a fixed set of ionospheric parameters H_{max} and B . There is no reason why these values should be constant throughout the view period. Figures 5 and 6 show the percentage discrepancy involved for these two passes if H_{max} and B take on different values. The zero percentage line (x-axis) is, of course, pertinent to the calibration technique as outlined in this article, i.e., with $H_{max} = 300$ km, $B = 39$ km, and $\chi = 0$ deg. As seen from the figures, the discrepancy at low elevation angles due to the variation of H_{max} can be more than 6% for both configurations, while that for the B variation is less than 1% for the Mariner 4 mission but can be more than 4% for the Mariner 5 mission. From Fig. 5, it is interesting to note that the sensitivity of the normalized ratios $R(\gamma)$, and therefore the range changes on the scale height B , is quite small even at low elevation angles, provided that the solar zenith angles are also small at the same time.

It should be noted that the curves in these figures are computed from a fixed maximum offset from the nominal values of the ionospheric parameters. Since these values vary during the view period and from day to day, the uncertainty in each pass resulting from this mapping technique is anywhere between the extrema of these curves. In other words, the uncertainties entailed are usually less than those indicated by the two outer-most curves.

E. Curve Fitting of One-Way Range Changes

The product delivered to the orbit determination program (ODP) from this calibration scheme is the one-way range change coefficients due to ionospheric effects. Thus, the one-way range values along the different lines of sight

to the spacecraft in a view period have to be fitted with a polynomial in time, and the ionospheric "Adjust Resid" coefficients are then handed over to the ODP. In these curve fittings, however, there may be some difficulty in deciding what the best order of the time polynomial would be. Of course, the optimal approach would be to supply the ODP with different sets of range coefficients resulting from fittings of different orders, obtain the state and/or station solutions from the ODP for each set, and then compare the sizes of the remaining O - C residuals. This approach will be applied and the sensitivity of the results on the different orders will be published in a different paper in the near future.

In the meantime, however, this comparison has been carried out in two different ways: (1) the capability of the different fitted curves to reproduce the actual one-way range changes, which is indicated by the standard deviation associated with each fitted curve; and (2) the consistency of the station location changes Δr_s and $\Delta \lambda$ as given by the different fitted curves. This second approach makes use of the Hamilton-Melbourne formulation for a single pass of the spacecraft (Ref. 1). Note, however, that since the solar zenith angle effect is not taken into account in the Chapman profiles in the present calibration scheme, the resultant station location changes may not be exact. Nevertheless, if the changes obtained from the different orders are consistent, the indication is that the one-way range coefficients are insensitive to any reasonable order of curve fitting. Now several other operations (steps 6, 7, and 8 in Fig. 1) have to be performed on the one-way range changes before the station location changes can be obtained and extra uncertainties may be introduced. However, as shown in the following section, the uncertainties resulting from these extra operations are negligibly small and are predominated by the order of the one-way range fit. Moreover, any extra uncertainties would only accentuate the discrepancies between the different fitting orders. This comparison is, therefore, a valid approach.

The Mariner 9 mission, tracked by DSS 14 in December 1971, has been calibrated for the ionosphere using this program with the one-way range values fitted to time polynomials of maximum orders of 5, 7, and 10. Note that fitting orders higher than ~ 10 are undesirable since the extra curvatures in the fitted curves are detrimental to the doppler curves. Besides, the ODP will smooth the range curves to some extent, thus effecting a lower order fit anyway. Figure 7 shows the standard deviations associated with the passes. Not only are the standard deviations small in magnitude (≤ 0.1 m), but also, for most of the time, the differences in these values between the three

different orders are quite small (< 0.05 m) as well. This is, of course, due to the usually rather smooth variations of the range points. Thus, the different orders are all good fits to the actual values. Moreover, as shown in Fig. 8, the station location changes are not very sensitive to the maximum order of the fit. A change of this order by a power of five results in a change in the monthly averaged standard deviations of 0.027 m, a change of Δr_s by about $\frac{1}{2}$ m, and a change of $\Delta\lambda$ by about 1 m *only* in a few days out of the whole month.

Thus, for reasonable orders of curve fitting, the one-way range coefficients are almost unaffected. The contribution from this operation to the total uncertainty is taken to be the largest of the three monthly averaged standard deviations, which in this case is the one with the lowest order of fit. This is root-sum-squared with the uncertainties introduced in the other steps and the RSS values (Table 1) are then the errors associated with the ionospheric one-way range coefficients delivered to the ODP.

F. Doppler Evaluation and Curve Fitting

As shown in Fig. 1, instead of supplying the ODP with the one-way range coefficients, this ionospheric calibration program also has the capability of doing the "four-path differencing" (Ref. 3) internally and then supplying coefficients of the resultant doppler, i.e., range rate, to the ODP. Although this mode of interface is seldom used at present, a brief analysis will be made for the sake of completeness.

Again, the analysis of this mode of operation can be made only in terms of station location changes without the detailed approach outlined in the preceding section involving the ODP. Moreover, since the solar zenith angle effect has not been taken into account in this scheme and the calibrations from the global model (Refs. 8 and 12) are not yet available for comparison, this is only a discussion on the general properties of the evaluation and fitting of the doppler effects. Data from Mariner 9 in December 1971 have been further analyzed in this connection.

Note that in order to get the station location changes due to the ionosphere from the one-way range corrections, the doppler points computed from the range curve have to be fitted with a time polynomial as well. This may introduce some error to the values of Δr_s and $\Delta\lambda$. However, since a high order (up to 19) polynomial has been used, the doppler points have been represented very well. The error caused by this second curve fitting to the station location changes should therefore be quite small.

A careful inspection of Fig. 8 and the associated range and doppler plots for the individual days reveals much more information about the evaluation of the range rate. Although the $\Delta\lambda$ solutions almost always agree quite well for the different maximum orders of the range fit polynomials, there are a few days when the low-order fit to the range curves gives $\Delta\lambda$ values that are different by more than a meter from the results of the higher order fit. Inevitably, this can be traced to the lower density of TEC data points in the pass, especially in the beginning and in the end. Thus, any variation in any one of these TEC points can greatly affect the shapes and phases of the different fitted curves. Consequently, the station location solutions are affected as well. Notice that data gaps close to the middle of the pass have little or no effect on these solutions. Note also that for an incomplete pass of only 4 or 5 h a very large error in $\Delta\lambda$ can result. The $\Delta\lambda$ solution of -7 m on December 7 has been omitted for this reason. Figures 9 and 10, which show the range and doppler curves on December 13 for two different fitting orders, serve to illustrate this point quite well.

IV. Conclusions

Table 1 shows a summary of all the one-way range change error sources and their magnitudes as a function of elevation angle in the ionospheric calibration technique as schematically outlined in Fig. 1. The RSS values are then the uncertainties associated with the ionospheric one-way range changes delivered to the ODP. Note that these are worst-case estimates, and the uncertainties encountered in this calibration technique are usually smaller. Whenever relevant, classifications according to seasons are also indicated. As mentioned, these uncertainties are primarily concerned with the daytime ionosphere. The worst-case total uncertainty is root-sum-squared and is also tabulated in Table 1. Although the two Mariner 4 and 5 passes worked out in detail here do not cover all possible solar zenith angle and elevation angle configurations, they are representative of all past planetary missions. Moreover, the analysis of this Mariner 5 configuration illustrates very well the amplification of the diurnal effect of the TEC by the elevation angle effect, as pointed out by Trask and Mulhall in Ref. 14.

Although at the expense of more tedious and time consuming programs, most of the sources of error in this ionospheric calibration scheme can be removed. However, before this can be pursued, the global ionospheric model developed by O. H. von Roos and the author, and which is valid both day and night, has to be checked out for its

sensitivities on the different model parameters and its feasibility of implementation. If improvements are to be obtained and implementation is found to be feasible, this

new model will replace the mapping scheme outlined here. Otherwise, improvement for this present technique will be implemented.

References

1. Hamilton, T. W., and Melbourne, W. G., "Information Content of a Single Pass of Doppler Data from a Distant Spacecraft," in *The Deep Space Network, Space Programs Summary 37-39*, Vol. III, pp. 18-23. Jet Propulsion Laboratory, Pasadena, Calif., May 31, 1966.
2. Mottinger, N. A., and Sjogren, W. L., "Station Locations," in *Tracking System Analytic Calibration Activities for the Mariner Mars 1969 Mission*, Technical Report 32-1499, pp. 19-34. Jet Propulsion Laboratory, Pasadena, Calif., Nov. 15, 1970.
3. Mulhall, B. D., Ondrasik, V. J., and Thuleen, K. L., "The Ionosphere," in *Tracking System Analytic Calibration Activities for the Mariner Mars 1969 Mission*, Technical Report 32-1499, pp. 45-68. Jet Propulsion Laboratory, Pasadena, Calif., Nov. 15, 1970.
4. Mulhall, B. D., *Mathematical Formulations for Ionospheric Calibration and Comparison, Part I: Ionospheric Data Pre-Processing*, IOM 391.3-529, Feb. 1972 (JPL internal document).
5. Yip, K. W., and Mulhall, B. D., *A Model for the Diurnal Variation of Ionospheric Total Electron Content*, TM 391-318, Apr. 1972 (JPL internal document).
6. Liu, A., and Cain, D., *Ionospheric Range and Angular Corrections*, TM 312-694, Mar. 1966 (JPL internal document).
7. Chapman, S., "The Absorption and Dissociative or Ionizing Effect of Monochromatic Radiation in an Atmosphere on a Rotating Earth," *Proc. Phys. Soc. (London)*, Vol. 43, p. 25, 1931.
8. von Roos, O. H., and Yip, K. W., "Derivation of a General Expression for Ionospheric Range Corrections Valid for Arbitrary Solar Zenith Angles, Azimuths, Elevation Angles and Station Locations," in *The Deep Space Network Progress Report*, Technical Report 32-1526, Vol. XI, pp. 53-61. Jet Propulsion Laboratory, Pasadena, Calif., Oct. 15, 1972.
9. Mulhall, B. D., and Yip, K. W., *High Frequency Fluctuations in the Earth's Ionosphere as Determined from Faraday Rotation Measurements*, IOM 391.3-568, May 1972 (JPL internal document).
10. Rishbeth, H., and Garriott, O. K., *Introduction to Ionospheric Physics*, p. 51, Academic Press, Inc., New York, 1969.
11. von Roos, O. H., and Yip, K. W., *Determination of the Total Electron Content from Faraday Rotation Measurements*, TM 391-330, May 1972 (JPL internal document).

References (contd)

12. von Roos, O. H., and Escobal, P. R., "A Global Model of the Earth's Ionosphere: The Nighttime Ionosphere," in *The Deep Space Network Progress Report*, Technical Report 32-1526, Vol. XV, pp. 32-47. Jet Propulsion Laboratory, Pasadena, Calif., June 15, 1973.
13. Yip, K. W., *A New Technique for Ionospheric Range Calculations*, TM 391-278, Feb. 1972 (JPL internal document).
14. Trask, D. W., and Mulhall, B. D., "Tracking System Analytic Calibration Description," in *Tracking System Analytic Calibration Activities for the Mariner Mars 1969 Mission*, Technical Report 32-1499, pp. 1-17. Jet Propulsion Laboratory, Pasadena, Calif., Nov. 15, 1970.

Table 1. Worst-case one-way range uncertainties

Elevation angle, deg	Faraday rotation, %	Slant to zenith TEC, %	Mapping, % ^a				Zenith to line-of-sight TEC, %		Time polynomial fit to one-way range, % ^a	RSS error in July, %			
			Local		Distant		Mariner 4 configuration	Mariner 5 configuration		Mariner 4 configuration		Mariner 5 configuration	
			July	Sept-Oct	July	Sept				Local	Distant	Local	Distant
							Mariner 4 configuration	Mariner 5 configuration					
0.83	2.0	2.0	0.5	0.3	7.7	4.1	7.9	—	2.0	8.4	11.4	—	—
3.36	2.0	2.0	0.5	0.3	7.7	4.1	7.3	10.3	2.0	7.9	11.0	10.7	13.2
5.00	2.0	2.0	0.5	0.3	7.7	4.1	7.0	9.6	2.0	7.6	10.8	10.0	12.7
10.00	2.0	2.0	0.5	0.3	7.7	4.1	5.8	7.6	2.0	6.5	10.0	8.1	11.2
15.00	2.0	2.0	0.5	0.3	7.7	4.1	4.4	5.6	2.0	5.3	9.3	6.3	9.9
20.00	2.0	2.0	0.5	0.3	7.7	4.1	3.1	4.1	2.0	4.2	8.7	5.0	9.1
25.00	2.0	2.0	0.5	0.3	7.7	4.1	2.2	3.0	2.0	3.6	8.5	4.1	8.7
30.00	2.0	2.0	0.5	0.3	7.7	4.1	1.6	2.1	2.0	3.3	8.3	3.5	8.4
40.00	2.0	2.0	0.5	0.3	7.7	4.1	1.0	1.1	2.0	3.0	8.2	3.0	8.2
50.00	2.0	2.0	0.5	0.3	7.7	4.1	0.7	0.7	2.0	3.0	8.2	3.0	8.2
60.00	2.0	2.0	0.5	0.3	7.7	4.1	—	0.4	2.0	—	—	2.9	8.2

^aAn average percentage based on an 8-h view period centered around noon local time and a zenith TEC value of 3×10^{17} electrons/m² (~4 m in S-band).

Table 2. Possible discrepancies in line-of-sight to zenith conversion of TEC

χ , deg ^a	γ , deg	Ray trace (1) ^b	Ray trace (2) ^b	Ray trace (3) ^b	Ray trace (4) ^b	Ray trace (5) ^b	$\cos \alpha$
18.2	35.5	0.6356	0.6285	0.6425	0.6340	0.6371	0.6357
13.6	35.5	0.6355	0.6284	0.6423	0.6339	0.6370	0.6357
15.7	35.5	0.6355	0.6284	0.6424	0.6339	0.6370	0.6357
21.1	35.5	0.6358	0.6286	0.6426	0.6341	0.6373	0.6357
30.7	35.5	0.6361	0.6290	0.6430	0.6344	0.6378	0.6357
40.3	35.5	0.6368	0.6297	0.6436	0.6349	0.6386	0.6357
65.8	35.5	0.6401	0.6332	0.6468	0.6374	0.6428	0.6357

^aFrom July 12, 1965 pass of Mariner 4 mission.

^bChapman ionospheric parameters:

$$N_{\max} = 5 \times 10^6 \text{ electrons/cm}^3$$

- | | | |
|--|--|--|
| (1) $H_{\max} = 300$ km
$B = 39$ km | (3) $H_{\max} = 350$ km
$B = 39$ km | (5) $H_{\max} = 300$ km
$B = 49$ km |
| (2) $H_{\max} = 250$ km
$B = 39$ km | (4) $H_{\max} = 300$ km
$B = 29$ km | |

Table 3. Possible discrepancies in line-of-sight to zenith conversion of TEC

χ , deg ^a	γ , deg	Ray trace (1) ^b	Ray trace (2) ^b	Ray trace (3) ^b	Ray trace (4) ^b	Ray trace (5) ^b	$\cos \alpha$
65.6	35.5	0.6401	0.6331	0.6468	0.6373	0.6427	0.6357
51.9	35.5	0.6379	0.6309	0.6447	0.6357	0.6400	0.6357
47.4	35.5	0.6374	0.6304	0.6442	0.6354	0.6394	0.6357
52.1	35.5	0.6380	0.6309	0.6447	0.6357	0.6401	0.6357
55.6	35.5	0.6384	0.6314	0.6452	0.6361	0.6406	0.6357
60.1	35.5	0.6391	0.6321	0.6458	0.6366	0.6415	0.6357

^aFrom October 18, 1967 pass of Mariner 5 mission.

^bChapman ionospheric parameters; see footnote b in Table 2.

Table 4. Ionospheric calibration configurations

(a) Mission: Mariner 4; DSS: 11; Date: 7/12/65; SEP = 78.1 deg

UT, hr	ϕ , deg ^a	χ , deg	γ , deg
19.06	345.9	18.2	0.83
19.81	357.15	13.6	9.95
20.23	3.45	13.6	14.88
20.62	9.30	15.7	19.46
21.25	18.75	21.15	26.69
22.11	31.65	30.7	35.78
22.91	43.65	40.25	43.06
25.00	75.0	65.75	51.90

(b) Mission: Mariner 5; DSS: 11; Date: 10/18/67; SEP = 48.2 deg

16.66	309.9	65.6	61.03
18.23	333.45	51.9	54.65
19.04	345.6	47.4	47.25
19.63	354.45	45.75	39.03
20.33	4.95	45.65	32.97
20.80	12.0	46.8	27.43
21.80	27.0	52.1	15.29
22.26	33.9	55.6	9.65
22.78	41.7	60.1	3.36

^a ϕ = local time reckoned from noon.

Table 5. Average discrepancy in local zenith TEC mapping between Stanford and Goldstone, Calif.

(a) Average discrepancy with time span centered at 12 noon		
Data span	$12.00^h \text{ (noon)} \pm 0.25^h$	$12.00^h \text{ (noon)} \pm 4.00^h$
July 1–31	$-0.09 \pm 0.20 \text{ meter (16)}^a$	$-0.02 \pm 0.21 \text{ meter (16)}^a$
Sept 12–Oct 12	$-0.02 \pm 0.39 \text{ meter (20)}^a$	$-0.01 \pm 0.34 \text{ meter (18)}^a$
(b) Average discrepancy with time span centered at 6 p.m.		
Data span	$6.00^h \text{ (p.m.)} \pm 0.25^h$	$6.00^h \text{ (p.m.)} \pm 4.00^h$
July 1–31	$0.00 \pm 0.25 \text{ meter (15)}^a$	$0.19 \pm 0.10 \text{ meter (11)}^a$
Sept 12–Oct 12	$0.16 \pm 0.36 \text{ meter (19)}^a$	$0.01 \pm 0.21 \text{ meter (14)}^a$

^aNumber of days in average.

Table 6. Average discrepancy in distant zenith TEC mapping between Hamilton, Mass., and Goldstone, Calif.

(a) Average discrepancy with time span centered at 12 noon		
Data span	$12.00^h \text{ (noon)} \pm 0.25^h$	$12.00^h \text{ (noon)} \pm 4.00^h$
July 1–31	$0.40 \pm 0.67 \text{ meter (19)}^a$	$0.30 \pm 0.61 \text{ meter (19)}^a$
Sept 12–30	$0.54 \pm 1.01 \text{ meter (11)}^a$	$0.16 \pm 0.46 \text{ meter (10)}^a$
(b) Average discrepancy with time span centered at 6 p.m.		
Data span	$6.00^h \text{ (p.m.)} \pm 0.25^h$	$6.00^h \text{ (p.m.)} \pm 4.00^h$
July 1–31	$-0.49 \pm 0.49 \text{ meter (18)}^a$	$-0.28 \pm 0.30 \text{ meter (15)}^a$
Sept 12–30	$0.90 \pm 1.20 \text{ meter (12)}^a$	$-0.83 \pm 0.55 \text{ meter (8)}^a$

^aNumber of days in average.

Table 7. Solar zenith angle effect on $\Delta\rho$ (γ) and R (γ)

(a) Mission: Mariner 4; DSS: 11; Date: 7/12/65; SEP = 78.1 deg						
γ , deg	Ray-trace solution with different χ values			Ray-trace solution with $\chi = 0$ deg		
	χ , deg	$\Delta\rho$, m	$R(\gamma)$	χ , deg	$\Delta\rho$, m	$R(\gamma)$
0.83	18.2	19.1747	} 3.1899	0	19.7289	} 3.1990
90.0	18.2	6.0111		0	6.1672	
9.95	13.6	17.1654	} 2.8232	0	17.4318	} 2.8265
90.0	13.6	6.0801		0	6.1672	
14.88	13.6	15.2724	} 2.5119	0	15.5049	} 2.5141
90.0	13.6	6.0801		0	6.1672	
19.46	15.7	13.5462	} 2.2386	0	13.8187	} 2.2407
90.0	15.7	6.0511		0	6.1672	
26.69	21.15	11.2166	} 1.8833	0	11.6266	} 1.8852
90.00	21.15	5.9559		0	6.1672	
35.78	30.7	8.9439	} 1.5640	0	9.6576	} 1.5660
90.0	30.7	5.7187		0	6.1672	
43.06	40.25	7.4628	} 1.3851	0	8.5546	} 1.3871
90.0	40.25	5.3878		0	6.1672	
51.90	65.75	4.8610	} 1.2299	0	7.6055	} 1.2332
90.0	65.75	3.9522		0	6.1672	

(b) Mission: Mariner 5; DSS: 11; Date: 10/18/67; SEP = 48.2 deg						
61.03	65.6	4.4565	} 1.1242	0	6.9428	} 1.1258
90.0	65.6	3.9640		0	6.1672	
54.65	51.9	5.7878	} 1.1947	0	7.3769	} 1.1962
90.0	51.9	4.8445		0	6.1672	
47.25	47.4	6.6201	} 1.3047	0	8.0596	} 1.3069
90.0	47.4	5.0739		0	6.1672	
39.03	45.75	7.6012	} 1.4755	0	9.1221	} 1.4791
90.0	45.75	5.1517		0	6.1672	
32.97	45.65	8.4865	} 1.6458	0	10.1862	} 1.6517
90.0	45.65	5.1564		0	6.1672	
27.43	46.8	9.4126	} 1.8447	0	11.4363	} 1.8544
90.0	46.8	5.1026		0	6.1672	
15.29	52.1	11.8539	} 2.4524	0	15.3456	} 2.4883
90.0	52.1	4.8337		0	6.1672	
9.65	55.6	12.8846	} 2.7795	0	17.5469	} 2.8452
90.0	55.6	4.6355		0	6.1672	
3.36	60.1	13.2401	} 3.0406	0	19.4331	} 3.1511
90.0	60.1	4.3544		0	6.1672	

Chapman ionospheric parameters: $N_{\max} = 5 \times 10^6$ electrons/cm³; $H_{\max} = 300$ km; $B = 39$ km.

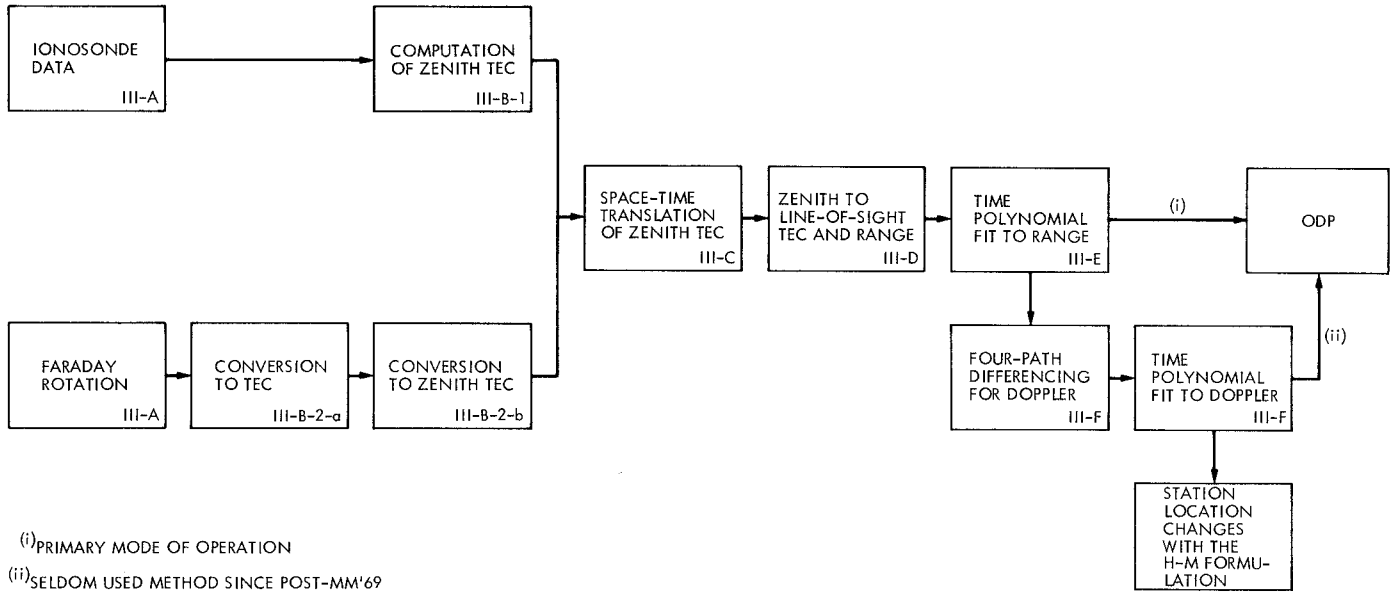


Fig. 1. Block diagram for an ionospheric calibration scheme

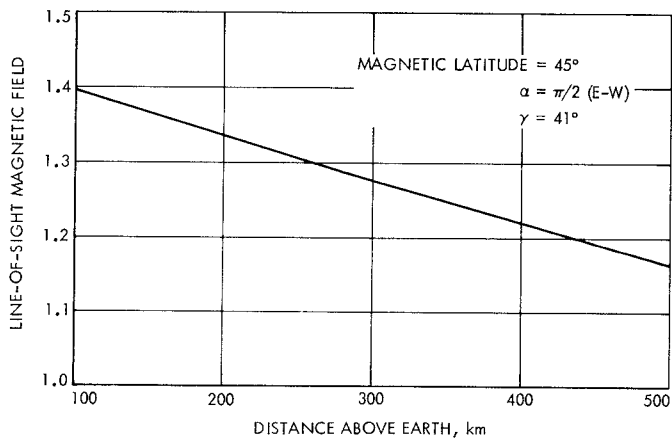


Fig. 2. Variation of line-of-sight magnetic field with geocentric distance in E-W direction

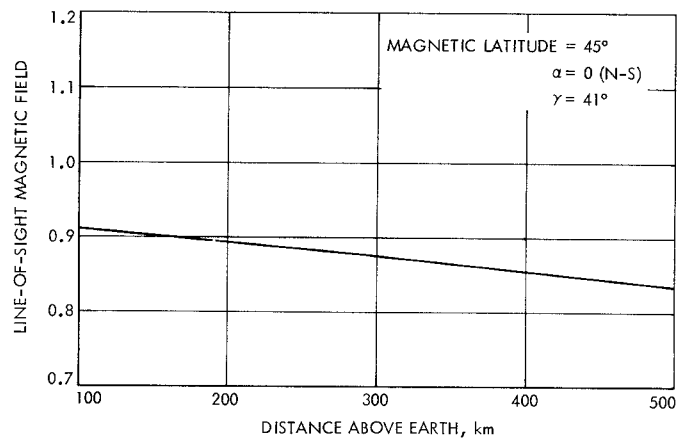
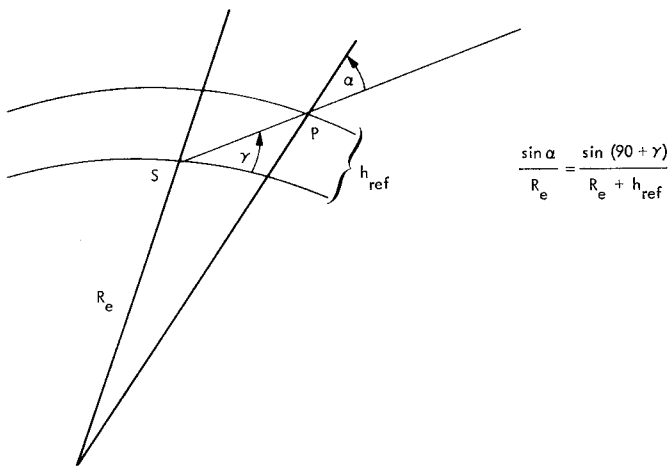


Fig. 3. Variation of line-of-sight magnetic field with geocentric distance in N-S direction



$$\frac{\sin \alpha}{R_e} = \frac{\sin (90 + \gamma)}{R_e + h_{ref}}$$

- γ = ELEVATION ANGLE OF RAY PATH TOWARD GEOSTATIONARY SATELLITE FROM OBSERVATORY S
- α = "REFERENCE ANGLE" BETWEEN RAY PATH AND ZENITH OF IONOSPHERIC REFERENCE POINT P
- h_{ref} = REFERENCE ALTITUDE, 350 km
- R_e = RADIUS OF EARTH

Fig. 4. Geometry of the ionospheric reference point P

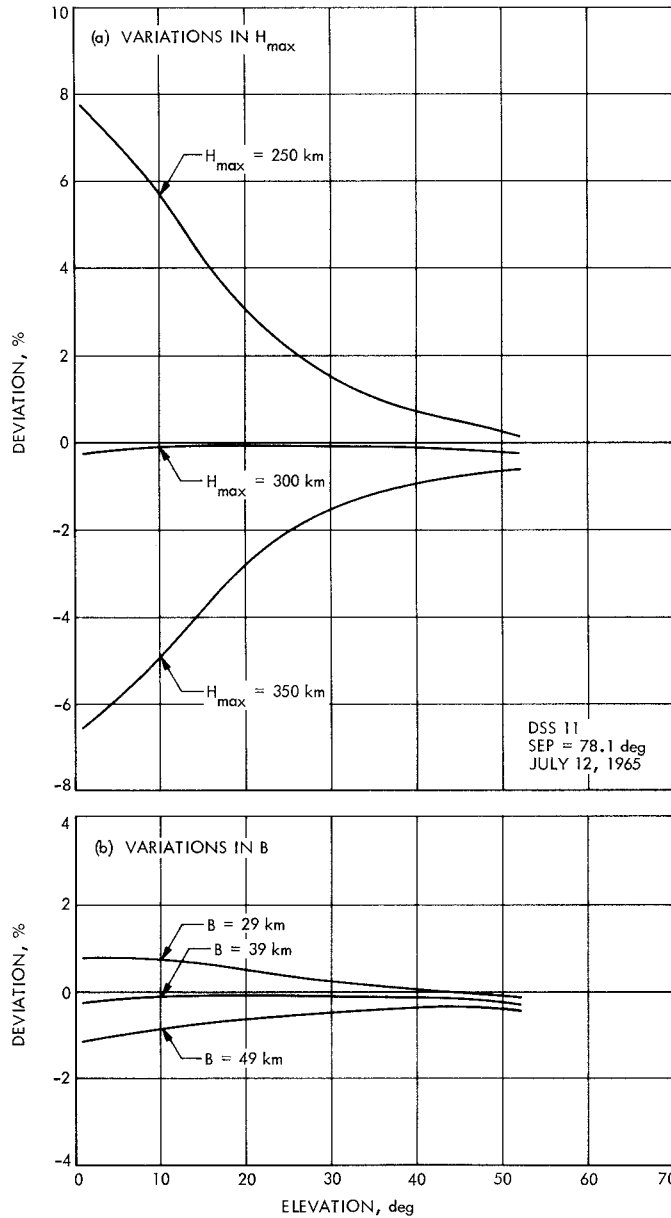


Fig. 5. Percentage discrepancy due to variations in H_{max} and B for the Mariner 4 pre-encounter configuration

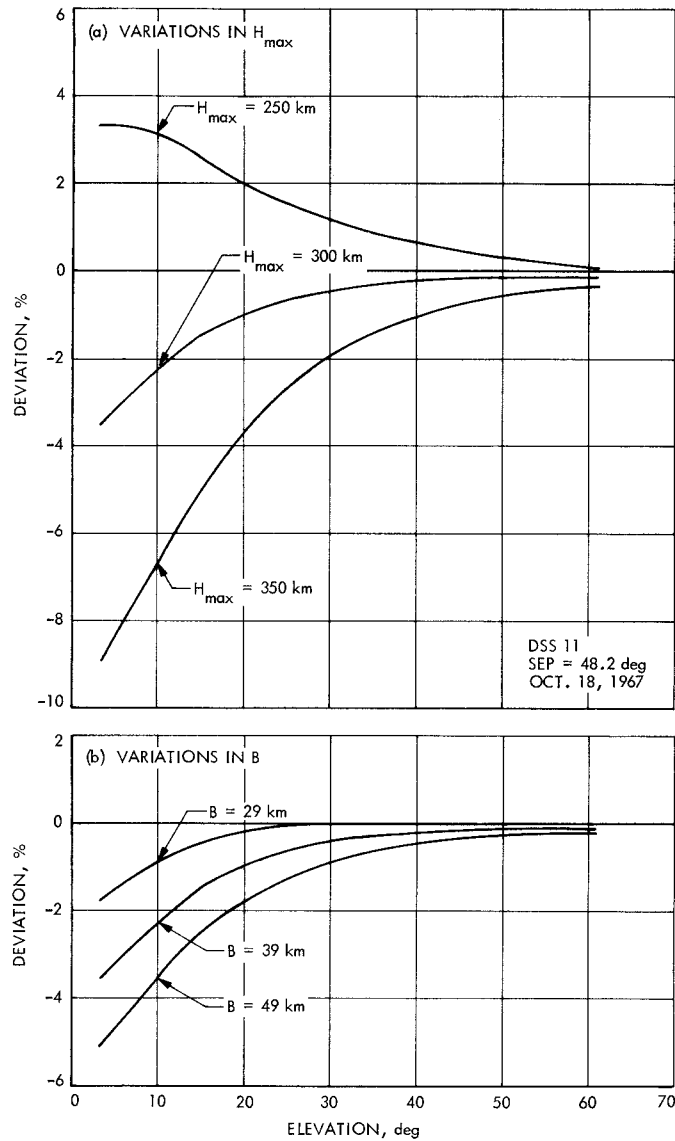


Fig. 6. Percentage discrepancy due to variations in H_{max} and B for the Mariner 5 pre-encounter configuration

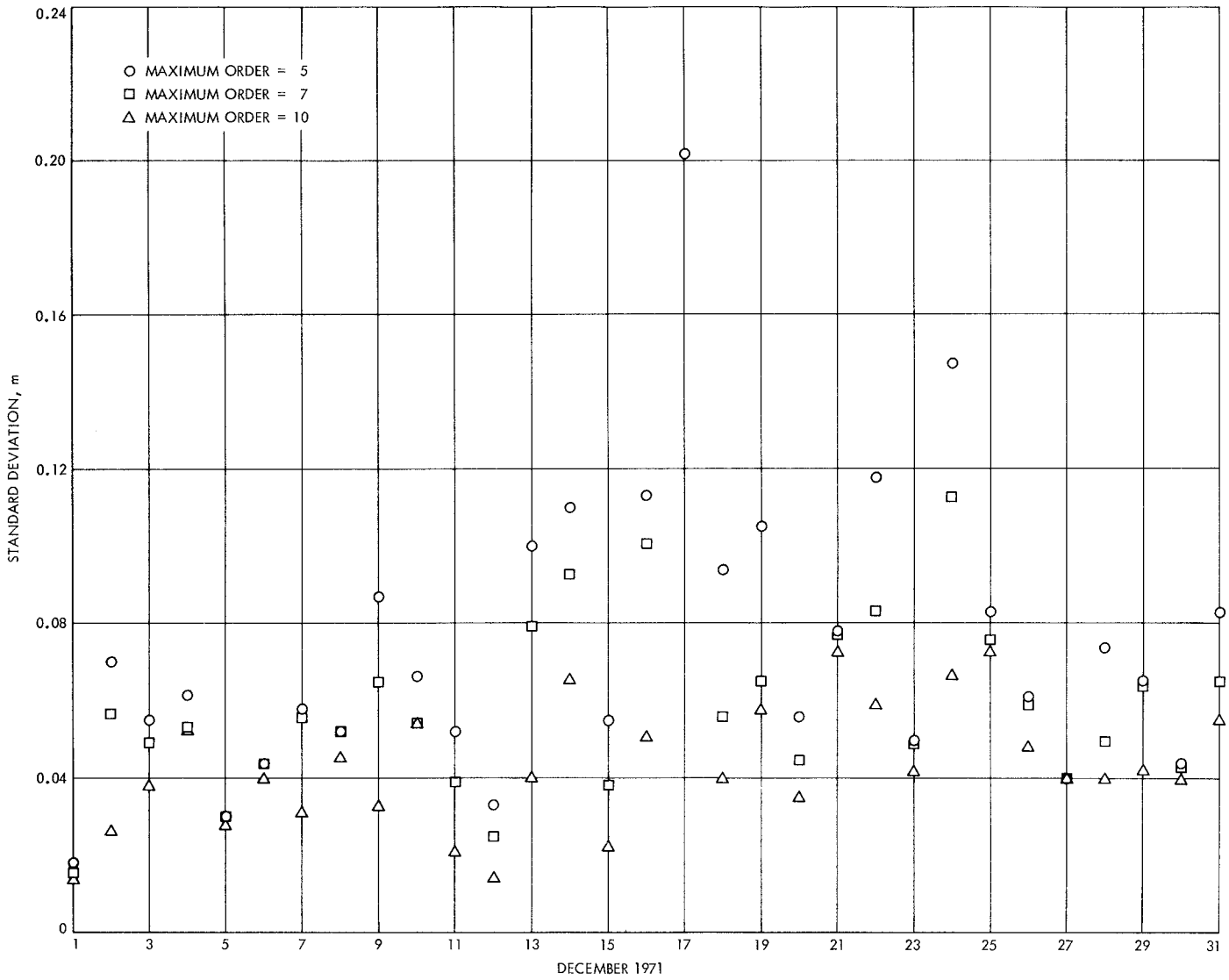


Fig. 7. Standard deviations from fitting of one-way range change

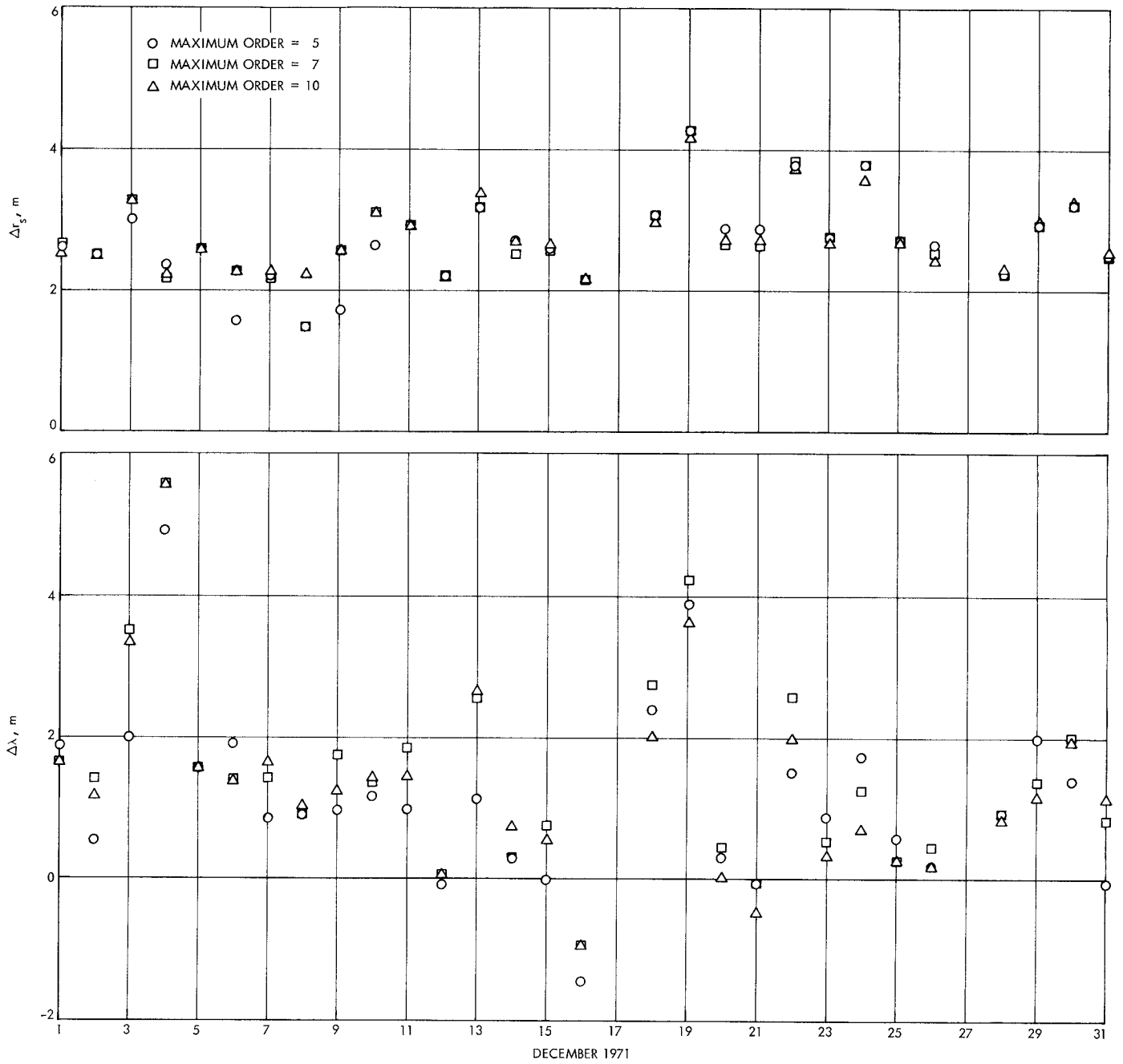


Fig. 8. Ionospheric station location changes for Mariner 9

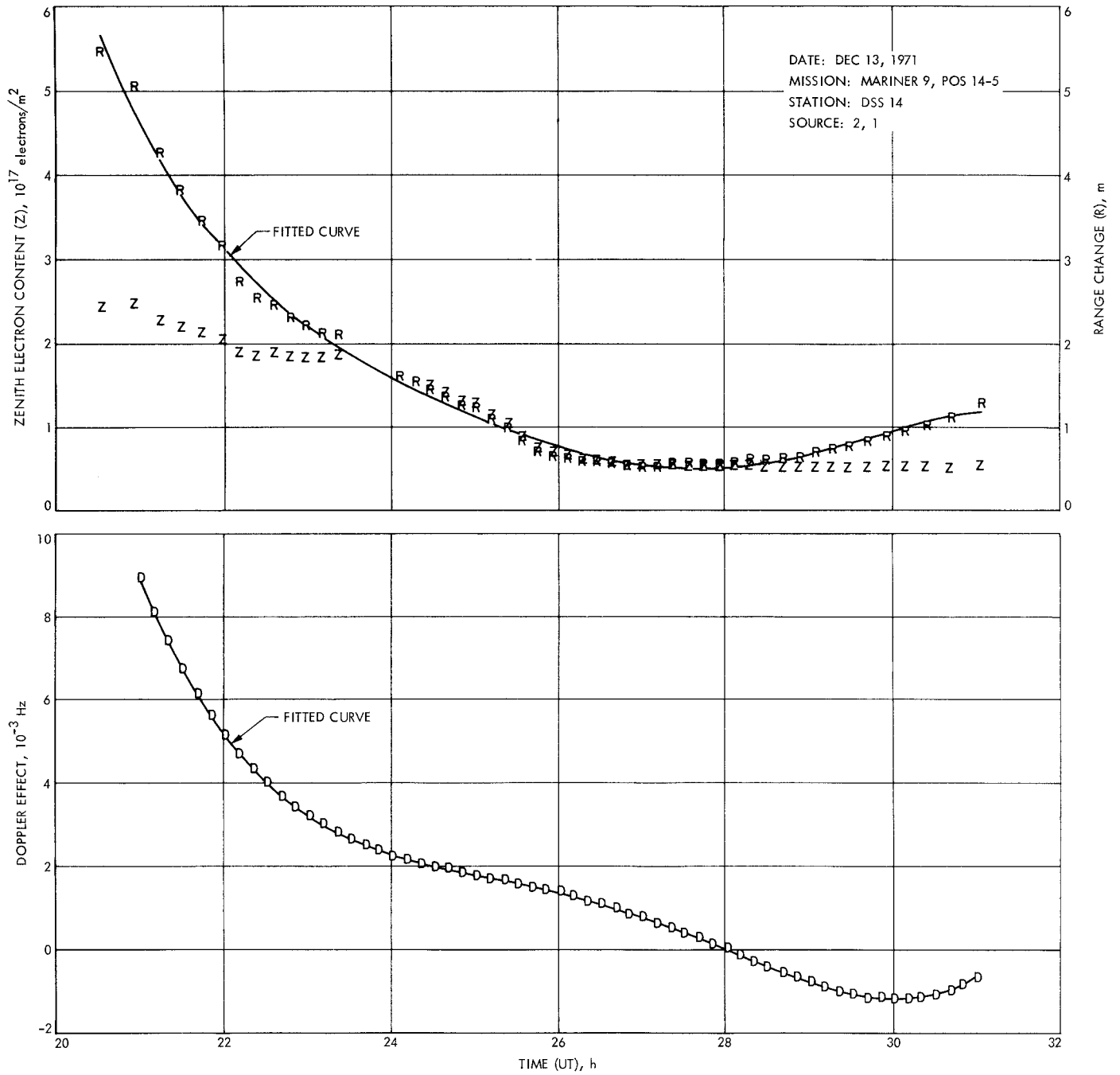


Fig. 9. Ionospheric range change and doppler effect for maximum order of range fit of 5

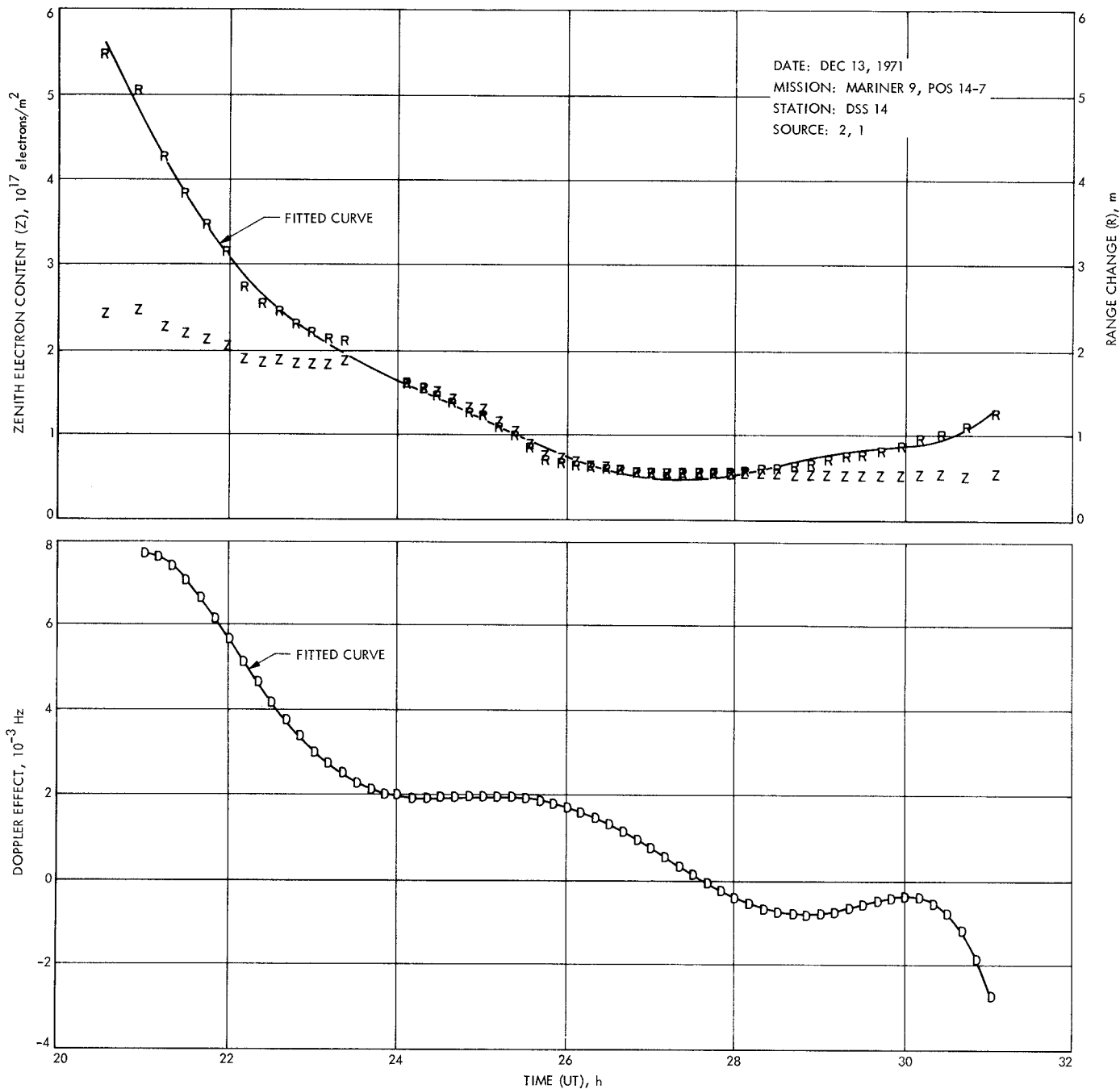


Fig. 10. Ionospheric range change and doppler effect for maximum order of range fit of 7